⑫

API-TR-127

RADAR CROSS-SECTION OF DAMPED CYLINDERS
AND DIELECTRIC STRIPS

Technical Progress Report

ITEM 0003

June 12, 1986

Prepared by

Richard Holland
Kah-Song Cho

for

Office of Naval Research

Under

Contract Number N00014-85-C-0852

S D E L E C T E D
JUN 1 9 1986
E

ap Applied Physics, Inc.

REPORT DOCUMENTATION PAGE

1a. REPORT SECURITY CLASSIFICATION	1b. RESTRICTIVE MARKINGS
Unclassified	APPROVED FOR PUBLIC RELEASE:

2a. SECURITY CLASSIFICATION AUTHORITY	3. DISTRIBUTION/AVAILABILITY OF REPORT
DARPA Technical Information Office	DISTRIBUTION IS UNLIMITED
2b. DECLASSIFICATION/DOWNGRADING SCHEDULE	
N/A	

4. PERFORMING ORGANIZATION REPORT NUMBER(S)	5. MONITORING ORGANIZATION REPORT NUMBER(S)
Technical Progress Report Item 0003 API-TR-127	

6a. NAME OF PERFORMING ORGANIZATION	6b. OFFICE SYMBOL (If applicable)	7a. NAME OF MONITORING ORGANIZATION
Applied Physics, Inc.		Office of Naval Research

6c. ADDRESS (City, State and ZIP Code)	7b. ADDRESS (City, State and ZIP Code)
5353 Wyoming Blvd., NE, Suite 3 Albuquerque, NM 87109	800 N. Quincy Street Arlington, VA 22217

8a. NAME OF FUNDING/SPONSORING ORGANIZATION	8b. OFFICE SYMBOL (If applicable)	9. PROCUREMENT INSTRUMENT IDENTIFICATION NUMBER
DARPA		N00014-85-C-0852

8c. ADDRESS (City, State and ZIP Code)	10. SOURCE OF FUNDING NUMBERS			
1400 Wilson Blvd. Arlington, VA 22209	PROGRAM ELEMENT NO.	PROJECT NO.	TASK NO.	WORK UNIT ACCESSION NO.

11. TITLE (Include Security Classification)

Radar Cross-Section of Damped Cylinders and Dielectric Strips

12. PERSONAL AUTHOR(S)

Richard Holland and Kah-Song Cho

13a. TYPE OF REPORT	13b. TIME COVERED	14. DATE OF REPORT (Year, Month, Day)	15. PAGE COUNT
Quarterly	FROM 3/86 TO 6/86	86 March 13	51

16. SUPPLEMENTARY NOTATION

17. COSATI CODES			18. SUBJECT TERMS (Continue on reverse if necessary and identify by block number)
FIELD	GROUP	SUB-GROUP	TDFD codes, echo widths, RCS calculation, stealth, dielectric strips

19. ABSTRACT (Continue on reverse if necessary and identify by block number)

(U)   This report presents 2D RCS (echo width) calculations for electrically and magnetically conducting circular cylinders with and without an electromagnetically damping coat. Similar calculations for dielectric cylinders and thin dielectric strips are also given. In all cases, results computed by our new TDFD code and transformed to the frequency domain are compared and overlaid with calculations performed directly in the frequency domain. Detailed preliminary documentation of the TDFD RCS code.

20. DISTRIBUTION/AVAILABILITY OF ABSTRACT	21. ABSTRACT SECURITY CLASSIFICATION
☐ UNCLASSIFIED/UNLIMITED ☒ SAME AS RPT. ☐ DTIC USERS	UNCLASSIFIED

22a. NAME OF RESPONSIBLE INDIVIDUAL	22b. TELEPHONE (Include Area Code)	22c. OFFICE SYMBOL

DD FORM 1473, 84 MAR   83 APR edition may be used until exhausted. All other editions are obsolete.

TECHNICAL PROGRESS REPORT

Contract Number N00014-85-C-0852

Radar Cross-Section of Damped Cylinders
and Dielectric Strips

Most of the basic logic in our TDFD RCS code was in place at the beginning of this quarter. Consequently, we have now directed our primary concern to

1) Improving the computer efficiency of the code.

2) Making changes which lead to increased accuracy.

3) Examining a second canonical problem, a thin dielectric strip, to verify further the code accuracy.

4) Making the code more user-friendly.

5) Documenting the TDFD RCS code.

By way of Item 2 above, we have recomputed the RCS of a perfectly conducting rod .5 m in radius, bare and covered by a damper .5 m thick. The damper is characterized as $\epsilon/\epsilon_0 = \mu/\mu_0 = 1$, $\sigma = \epsilon\sigma^*/\mu = 4 \times 10^{-3}$. These values were selected to give a skin depth on the order of damper thickness at the frequencies (50 - 500 MHz) for which the calculations were run. The TDFD code utilized square cells 4 cm on a side or 25 cells to a cylinder diameter.

While our TDFD code only treats the TM case, we are able to simulate TE problems by use of duality. In particular, the above-described case was rerun with the cylinder perfectly magnetically conducting ($\sigma^* = \infty$, $\sigma = 0$), and the damper unchanged. The RCS obtained in this manner for TM illumination is the same as one would obtain for TE illumination of an ordinary electrically conducting rod.

Figures 1 and 2 show our TDFD RCS calculations for the damped and undamped electrically conducting rod. Overlaid on these figures are analytic solutions to the same problem as determined by expansion in

1
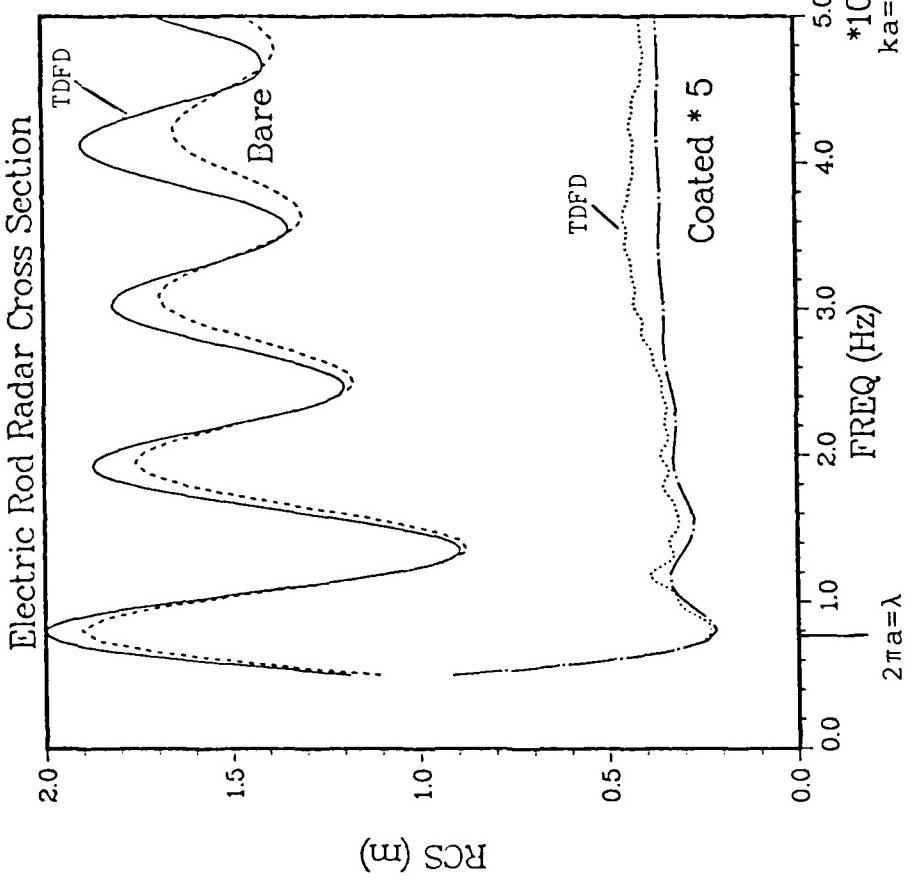
Figure 1. Echo width of bare and damped electrically conducting cylinder with E transverse to cylinder axis.
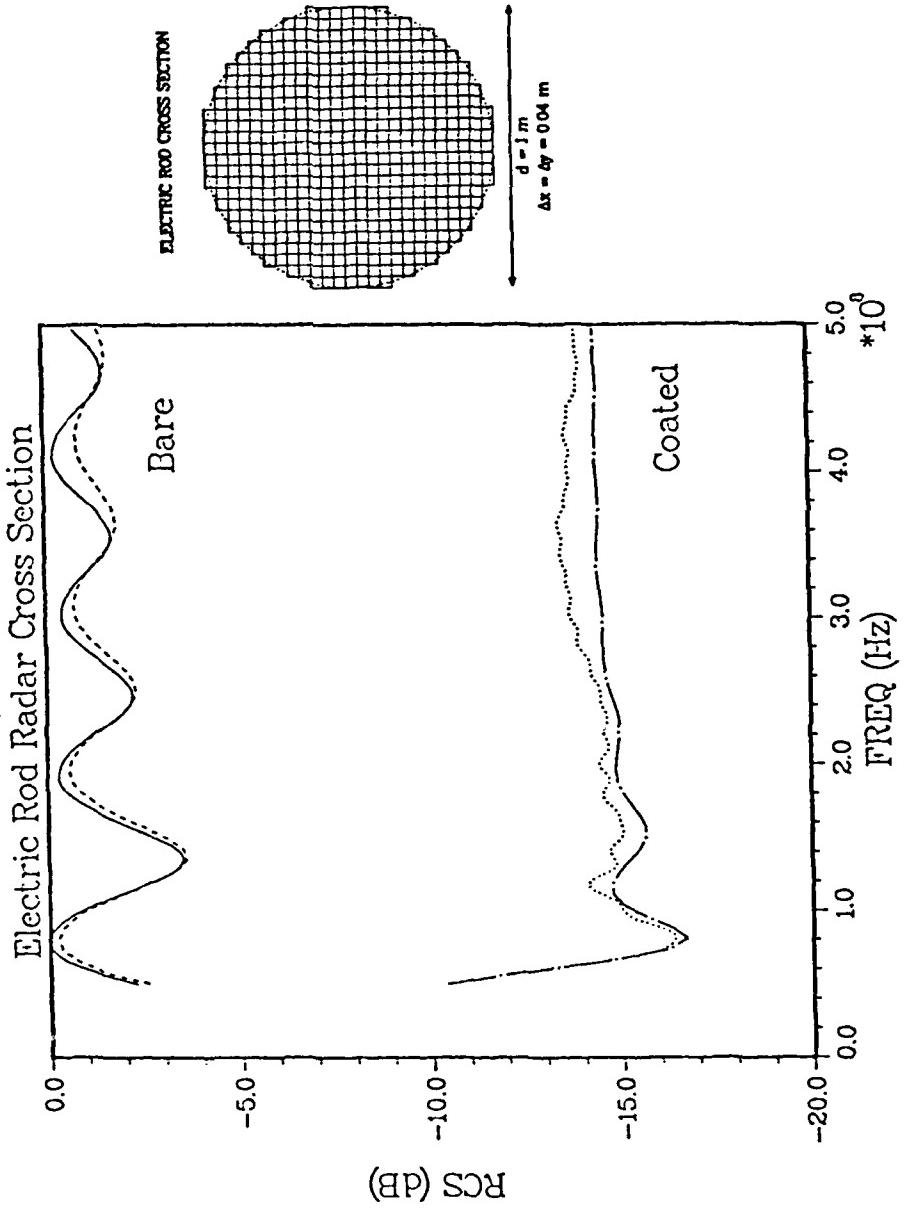
Figure 2. Echo width of bare and damped electrically conducting cylinder with E transverse to cylinder axis.

3

cylindrical harmonics (see the previous quarterly report for details of the harmonic expansion). These results should be compared with Figures 1 and 3 of the previous quarterly report. As one can see, the frequency-domain ripple which had been present on the response of the damped rod is now gone. This ripple had occurred because the outer boundary of the problem space was somewhat reflective. Hence, the true solution was "beating" with a coherent, but specious, echo. We have now found a way to implement a much less reflective outer boundary.

(Unlike 3D problems, we have empirically learned that 2D outer boundaries are least reflective if a pure radiating condition,

$$f(\underline{r}, t) \to g(t - r/c)/\sqrt{r}$$

is used without a damper inside the boundary. In conjunction with this outer boundary, the 2D code should not be run with Δt at the Courant limit, $\Delta s/(\sqrt{2}c)$, but at $\Delta s/(2c)$. This empirically discovered combination gives less outer-boundary reflection than an impedance boundary, a damped boundary, a pure $r^{-1/2}$ boundary, a Mur boundary, or any other mixture of the above.)

Figures 3 and 4 show our TDFD RCS calculation for the TE simulation. Again, these results are overlaid with the cylindrical-harmonic solution. These curves correspond to Figures 2 and 4 of the previous quarterly report. Again, the new results may be seen to be much "cleaner".

This improvement was obtained using the same techniques as the TM case, but with an additional twist. In retrospect, it is obvious that a perfectly conducting infinite rod illuminated by a unipolar EMP polarized along the rod axis will carry a d.c. response forever. If the EMP calculation of this response is stopped suddenly at t_0, the frequency transform of the result will be the true transform frequency-convolved with $\sin(\omega t_0/2)/(\omega t_0/2)$. We are now running the TE-like TDFD calculation long enough that $2/t_0$ is

4
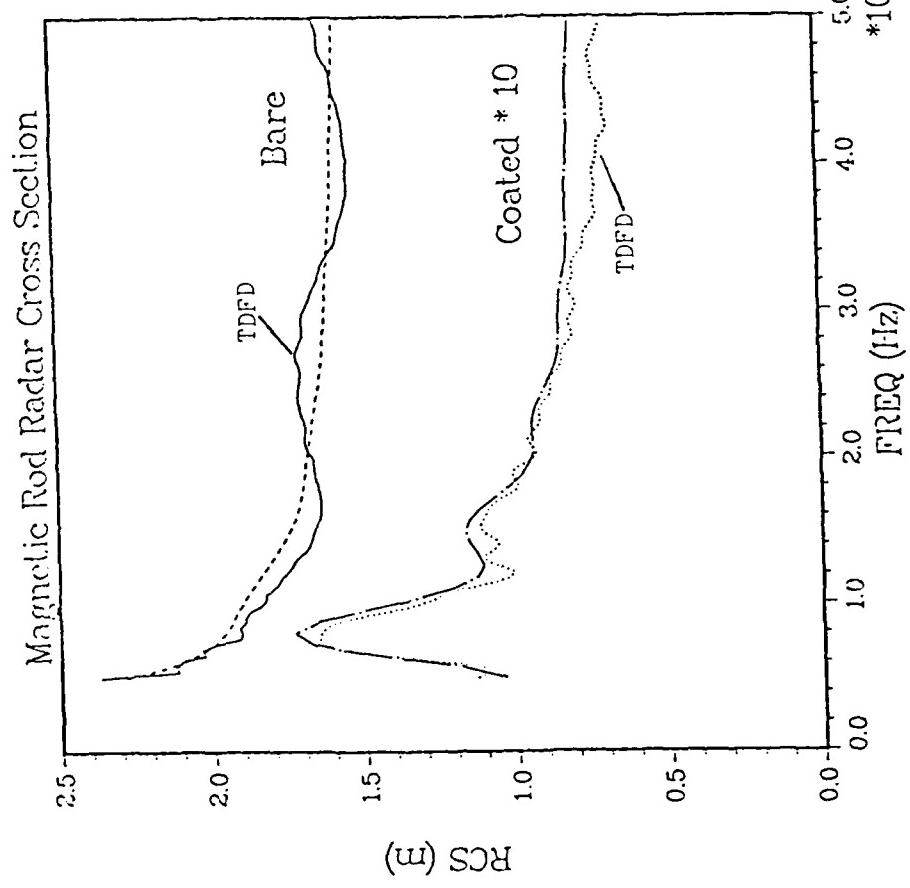
Figure 3. Echo width of bare and damped magnetically conducting cylinder with H parallel to cylinder axis.

5
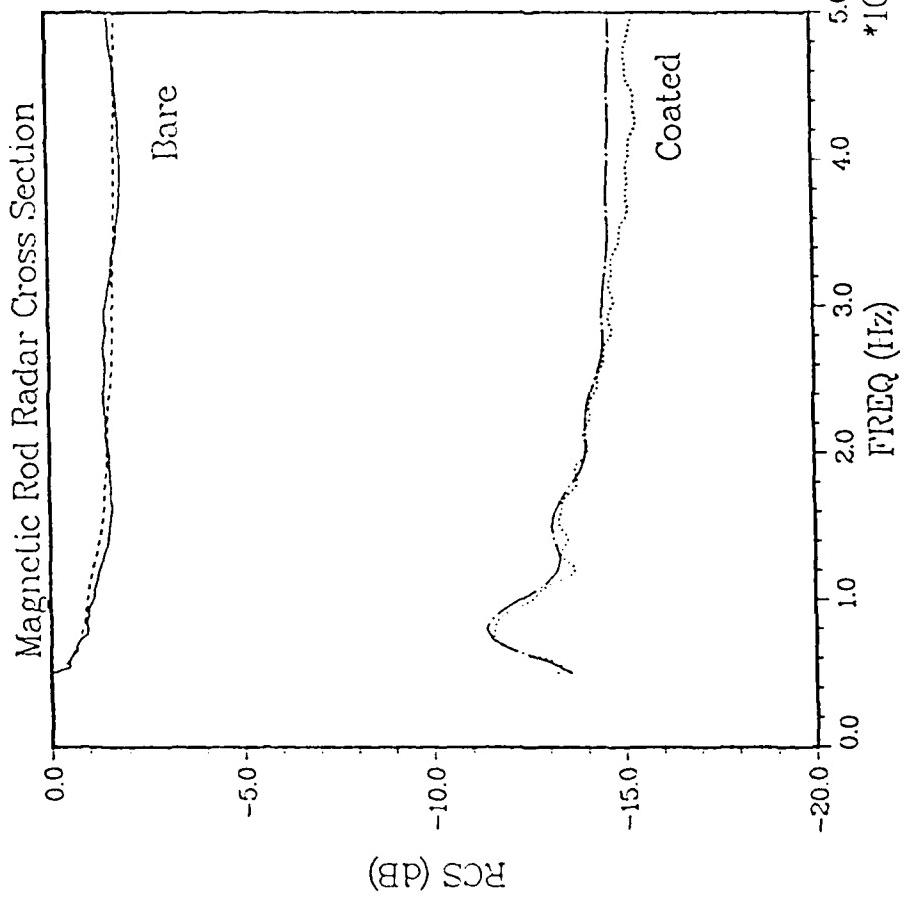
Figure 4. Echo width of bare and damped magnetically conducting cylinder with II parallel to cylinder axis.

smaller than any angular frequency of interest and then turning the code off "softly", say over 425 cycles.

Additionally, we now have results for scattering from dielectric cylinders .5 m in radius and characterized by $\epsilon/\epsilon_0 = 2$ or 9. (There is a fundamental difference between these two cases. At $\epsilon = 2\epsilon_0$, the optically shortest path from one side of the cylinder to the other is through the diameter. At $\epsilon = 9\epsilon_0$, it is around the circumference.) Figures 5-7 show overlays of these calculations and the harmonic expansion. It may be seen that the overlays begin to diverge above 300 MHz, especially for the $\epsilon = 9$ case. This corresponds to about 8 cells per wavelength.

Consequently, the dielectric cylinder calculations were rerun with Δs reduced from 4 cm to 2 cm. Figures 8-10 show the overlays based on the reduced Δs. These new results are considerably improved, especially at the higher frequencies.

It is our belief that, although great improvement has been achieved over the past quarter, we are still quite far from achieving the ultimate accuracy TDFD can provide. We especially hold this opinion with respect to eliminating the broad frequency-domain ripple appearing on our latest calculations for the bare-rod TE simulation.

Figures 11 and 12 present overlays for the second canonical problem, Item 3, TM scattering off a dielectric strip .025 m thick, 2 m wide, and characterized by $\sigma = 0$, $\epsilon_r = 2$. This data represents the monostatic RCS for a 45° angle of illumination with respect to the strip's major faces. The TDFD curves in these figures are based on 4 cm square cells. At the higher frequencies, 2 cm cells would doubtless improve the code-code agreement. The frequency-domain calculation is not strictly canonical, but is actually a modified Galerkin solution with three complex waves included to represent the strip behavior in the width direction. This frequency-domain solution is due to Richmond, and was brought to our attention by Dr. Stovall.

With respect to Item 4, we have now implemented some user-friendly graphics so the worker has a visual representation of the problem being

7
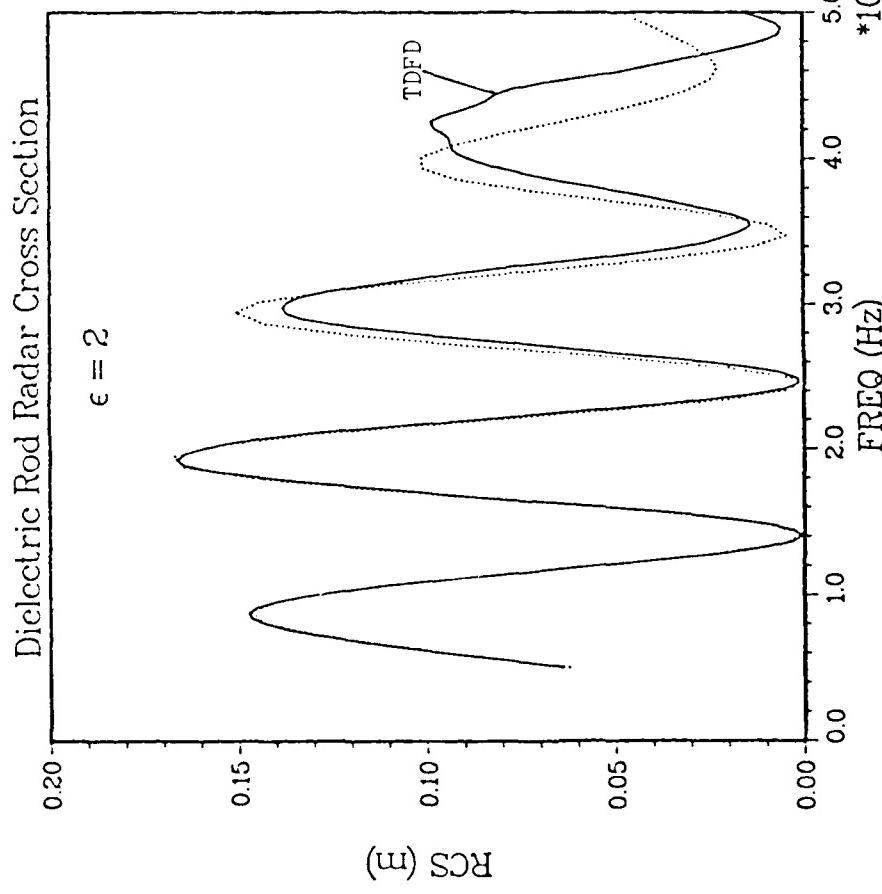
Figure 5. Echo width of a dielectric rod with E transverse to the rod axis. Based on rod diameter of 1 m and cells .04 m on a side.

8
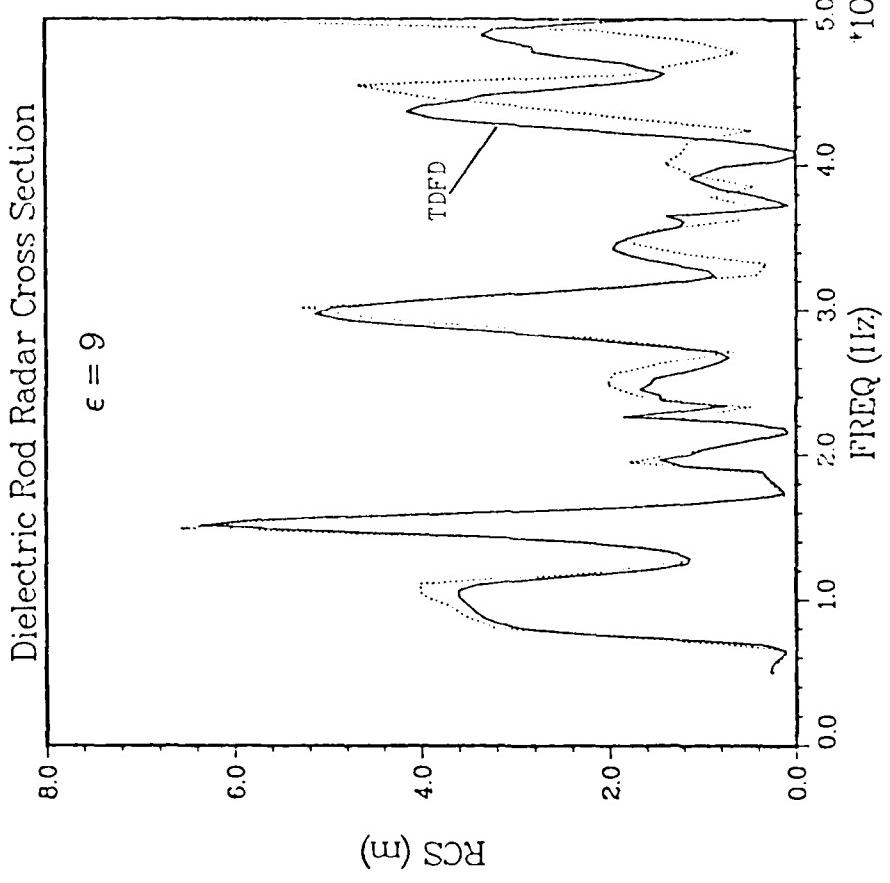
Figure 6. Echo width of a dielectric rod with E transverse to the rod axis. Based on rod diameter of 1 m and cells .04 m on a side.

9
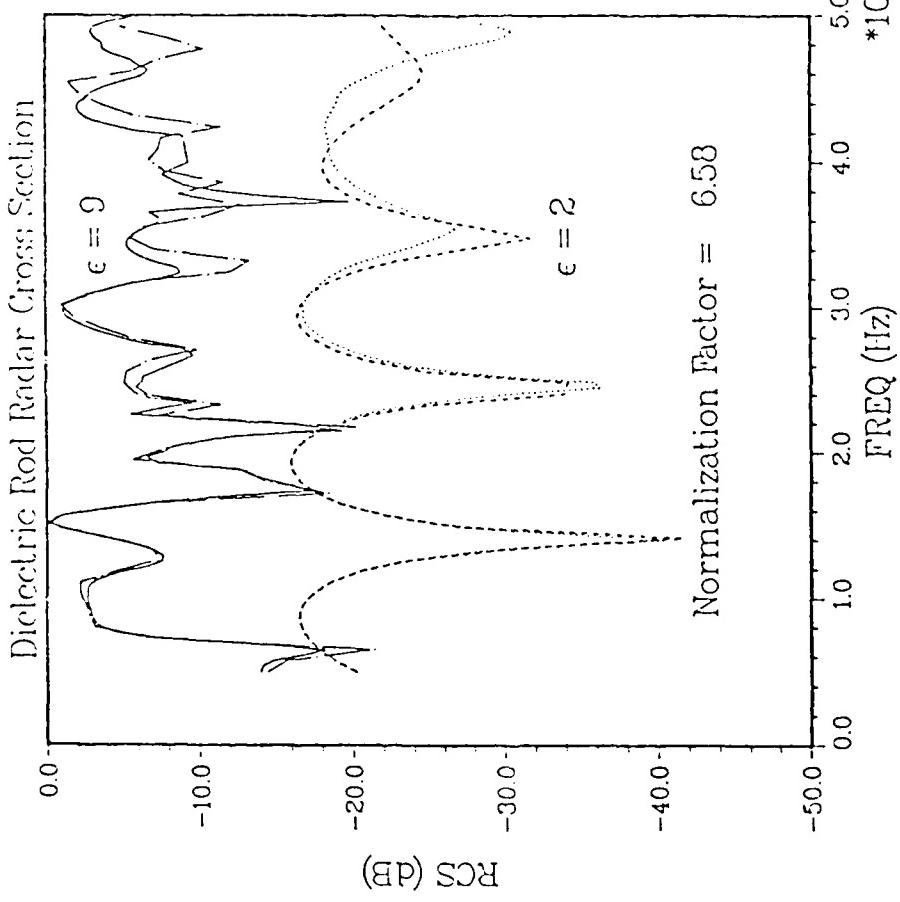
Figure 7. Echo width of a dielectric rod with E transverse to the rod axis. Based on rod diameter of 1 m and cells .04 m on a side.

10
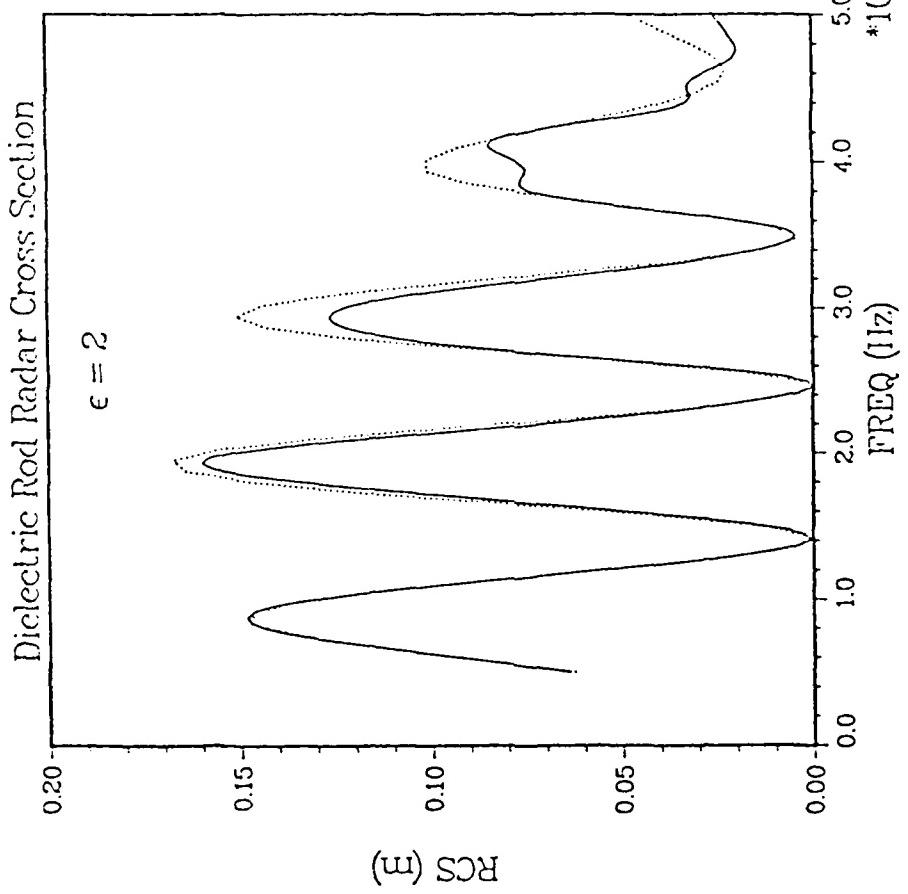
Figure 8. Echo width of a dielectric rod with E transverse to the rod axis. Based on rod diameter of 1 m and cells .02 m on a side.

11
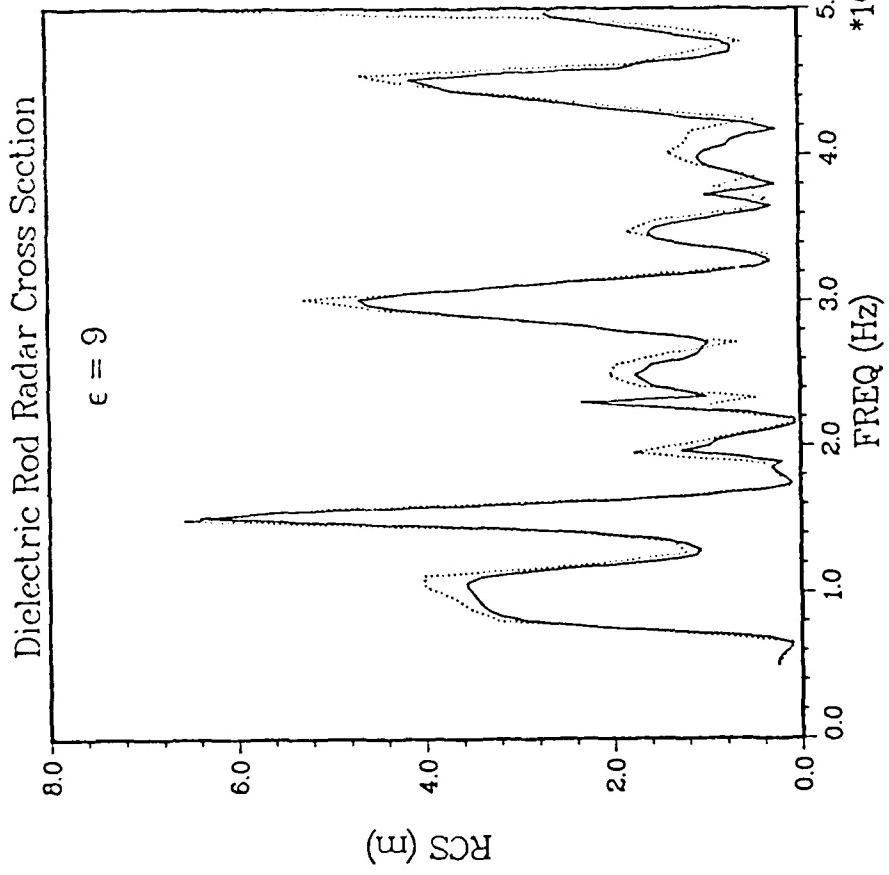
Figure 9.   Echo width of a dielectric rod with E transverse to the rod axis. Based on rod diameter of 1 m and cells .02 m on a side.

12
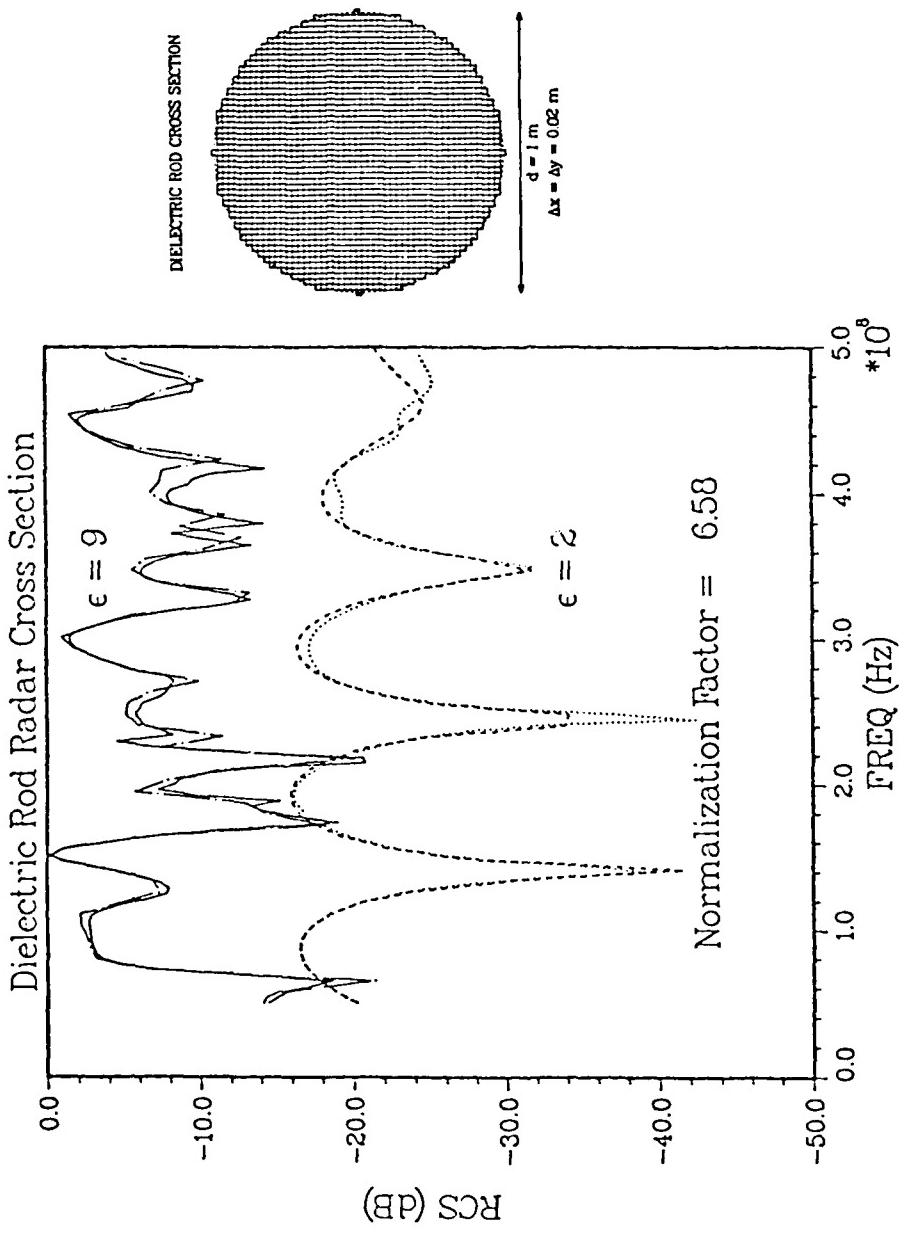
Figure 10. Echo width of a dielectric rod with E transverse to the rod axis. Based on a rod diameter of 1 m and cells .02 m on a side.
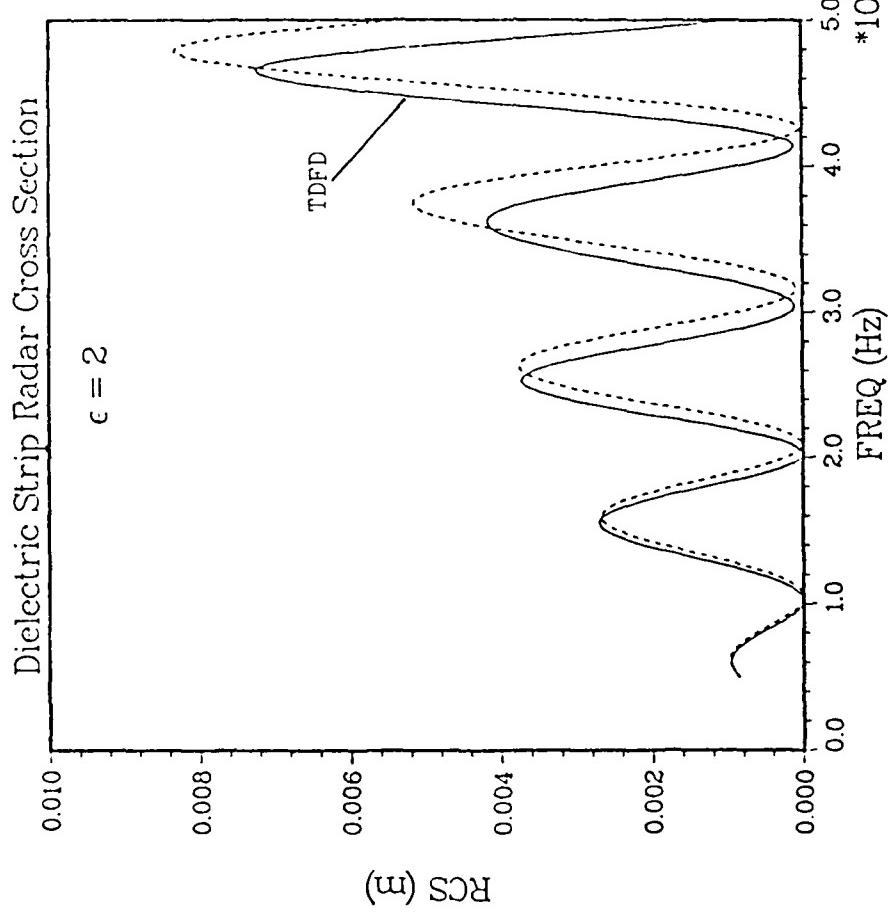
Figure 11. Echo width of a dielectric strip with E transverse to the strip axis. Based on a 45° angle of illumination, a strip .04 m x 2 m, and cells .04 m on a side.

14
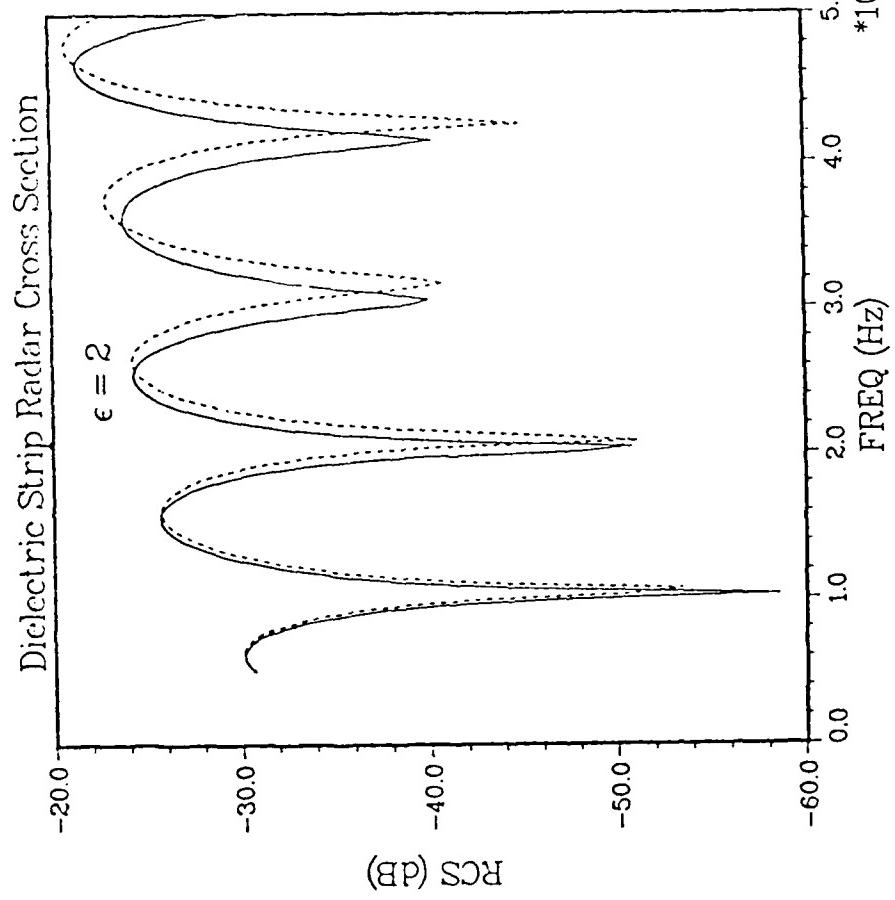
Figure 12. Echo width of a dielectric strip with E transverse to the strip axis. Based on a 45° angle of illumination, a strip .04 x 2 m, and cells .04 m on a side.

15

DAMPED ROD CROSS SECTION

d = 2 m

d = 1 m

$\Delta x = \Delta y = 0.04$ m
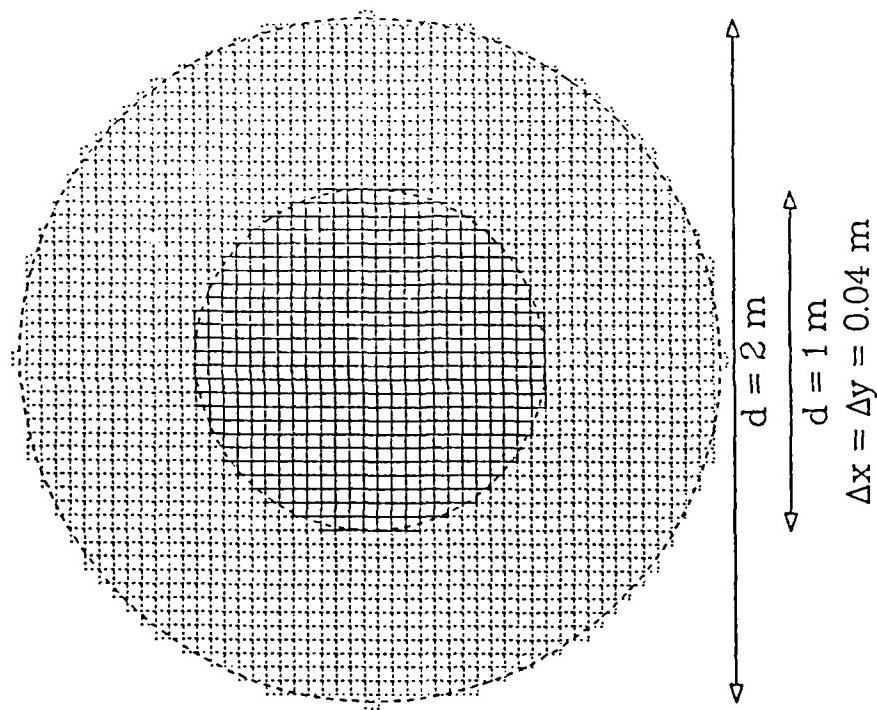
Figure 13. Finite-difference model of conducting rod 1 m in diameter coated by a damper of 2 m outer diameter. Figures 1 and 2 are based on this model.

16

solved.   For example, Figure 13 illustrates the cell occupancy by conductor
or damper for the damped electrically conducting rod upon which Figures 1
and 2 are based.

Lastly,   there   is   Item   5, the matter of TDFD RCS code documentation.
The remaining pages of this report constitute our first draft of this task.

Architecture of the Time-Domain Finite-Difference RCS Code

Equations to be Solved

We assume in this study that electromagnetically linear conditions prevail. Then the total field can be separated into an incident field (which would be the field in the absence of the scatterer) and a scattered field (the field modification caused by the scatterer's presence):

$$(\underline{E}^{T}, \underline{H}^{T}) = (\underline{E}^{inc}, \underline{H}^{inc}) + (\underline{E}^{scat}, \underline{H}^{scat}) \tag{1}$$

Under the linearity assumption, both the incident and the scattered fields individually satisfy Maxwell's equations.

If some background dissipation (σ_b, σ_b^*) is present, the incident fields will obey

$$\nabla \times \underline{E}^{inc} = - \mu_0 \frac{\partial \underline{H}^{inc}}{\partial t} - \sigma_b^* \underline{H}^{inc} \tag{2}$$

$$\nabla \times \underline{H}^{inc} = \epsilon_0 \frac{\partial \underline{E}^{inc}}{\partial t} + \sigma_b \underline{E}^{inc} \tag{3}$$

In the presence of an anisotropic scatterer with frequency dependent properties, the total fields conform to

$$\nabla \times \underline{E}^{T} = - \underline{\mu}_\infty \cdot \frac{\partial \underline{H}^{T}}{\partial t} - \underline{\sigma}_0^* \cdot \underline{H}^{T} - \int_{-\infty}^{t} \underline{K}^*(t-t') \cdot \frac{\partial \underline{H}^{T}(t')}{\partial t'} dt' - \underline{J}_f^* \tag{4}$$

18

$$\nabla \times \underline{H}^T = \underline{\underline{\epsilon}}_\infty \cdot \frac{\partial \underline{E}^T}{\partial t} + \underline{\underline{\sigma}}_0 \cdot \underline{E}^T + \int_{-\infty}^t \underline{\underline{K}}(t-t') \cdot \frac{\partial \underline{E}^T(t')}{\partial t'} dt' + \underline{J}_f \qquad (5)$$

Subtraction of the first pair of equations from the second leaves us with the version of Maxwell's equations obeyed by the scattered fields:

$$\nabla \times \underline{E}^{scat} = -\underline{\underline{\mu}}_\infty \cdot \frac{\partial \underline{H}^{scat}}{\partial t} - \underline{\underline{\sigma}}_0^* \cdot \underline{H}^{scat} - \int_{-\infty}^t \underline{\underline{K}}^*(t-t') \cdot \frac{\partial \underline{H}^{scat}(t')}{\partial t'} dt'$$

$$- (\underline{\underline{\mu}}_\infty - \underline{\underline{I}}\mu_0) \cdot \frac{\partial \underline{H}^{inc}}{\partial t} - (\underline{\underline{\sigma}}_0^* - \underline{\underline{I}}\sigma_b^*) \cdot \underline{H}^{inc} - \int_{-\infty}^t \underline{\underline{K}}^*(t-t') \cdot \frac{\partial \underline{H}^{inc}(t')}{\partial t'} dt'$$

$$- \underline{J}_f^* \qquad (6)$$

$$\nabla \times \underline{H}^{scat} = \underline{\underline{\epsilon}}_\infty \cdot \frac{\partial \underline{E}^{scat}}{\partial t} + \underline{\underline{\sigma}}_0 \cdot \underline{E}^{scat} + \int_{-\infty}^t \underline{\underline{K}}(t-t') \cdot \frac{\partial \underline{E}^{scat}(t')}{\partial t'} dt'$$

$$+ (\underline{\underline{\epsilon}}_\infty - \underline{\underline{I}}\epsilon_0) \cdot \frac{\partial \underline{E}^{inc}}{\partial t} + (\underline{\underline{\sigma}}_0 - \underline{\underline{I}}\sigma_b) \cdot \underline{E}^{inc} + \int_{-\infty}^t \underline{\underline{K}}(t-t') \cdot \frac{\partial \underline{E}^{inc}(t')}{\partial t'} dt'$$

$$+ \underline{J}_f \qquad (7)$$

It is convenient to represent the inhomogeneous parts (or incident parts) of eqs. (6) and (7) as

$$[J^{T*}] = -[\sigma_0^*][H^S] + [J_f^*] + [\nabla \times \underline{E}^{scat}] =$$

$$+ [\mu_\infty - \mu_0][\dot{H}^{inc}] + [\sigma_0^* - \sigma_b^*][H^{inc}]$$

$$+ \int_{-\infty}^{t}[K^*(t-t')][\dot{H}^{inc}(t')]dt' + [J_f^*] + [\nabla \times \underline{E}^{scat}] \qquad (8)$$

$$[J^T] = - [\sigma_0][E^S] + [J_f] - [\nabla \times \underline{H}^{scat}] =$$

$$+ [\epsilon_\infty - \epsilon_0][\dot{E}^{inc}] + [\sigma_0 - \sigma_b][E^{inc}]$$

$$+ \int_{-\infty}^{t}[K(t-t')][\dot{E}^{inc}(t')]dt' + [J_f] - [\nabla \times \underline{H}^{scat}] \qquad (9)$$

Thus, $[H^S]$ and $[E^S]$ become

$$[H^S] = - [\tau^*][\dot{H}^{inc}] - [R^*][H^{inc}] - \int_{-\infty}^{t}[A^*(t-t')][\dot{H}^{inc}(t')]dt' \qquad (10)$$

$$[E^S] = - [\tau][\dot{E}^{inc}] - [R][E^{inc}] - \int_{-\infty}^{t}[A(t-t')][\dot{E}^{inc}(t')]dt' \qquad (11)$$

In the last pair of equations, we have defined

$$[\tau^*] = [\sigma_0^*]^{-1}[\mu_\infty - \mu_0] \qquad (12)$$

$$[R^*] = [\sigma_0^*]^{-1}[\sigma_0^* - \sigma_b^*] \qquad (13)$$

20

$$[A^*] = [\sigma_0^*]^{-1}[K^*] \tag{14}$$

$$[\tau] = [\sigma_0]^{-1}[\epsilon_\infty - \epsilon_0] \tag{15}$$

$$[R] = [\sigma_0]^{-1}[\sigma_r - \sigma_b] \tag{16}$$

$$[A] = [\sigma_0]^{-1}[K] \tag{17}$$

Substituting eqs. (8) - (17) back into (6) and (7) yields

$$\underline{\underline{\mu}}_\infty \cdot \frac{\partial \underline{H}^{scat}}{\partial t} + \underline{\underline{\sigma}}_0^* \cdot \underline{H}^{scat} + \int_\infty^t \underline{\underline{K}}^*(t-t') \cdot \frac{\partial \underline{H}^{scat}(t')}{\partial t'} \, dt' = - \underline{J}^{T*} \tag{18}$$

$$\underline{\underline{\epsilon}}_\infty \cdot \frac{\partial \underline{E}^{scat}}{\partial t} + \underline{\underline{\sigma}}_0 \cdot \underline{E}^{scat} + \int_\infty^t \underline{\underline{K}}(t-t') \cdot \frac{\partial \underline{E}^{scat}(t')}{\partial t'} \, dt' = - \underline{J}^T \tag{19}$$

These are the scattered field equations we will be treating.

21

Method of Solution

For now, we shall only concern ourselves with the 2D TM case. Thus, E_x, E_y and H_z will be present. Equation (18) reduces to a scalar equation, but (19) remains a two-component vector equation.

Figure 14 illustrates a typical TDFD 2D unit cell, and shows where the three field components associated with that cell are located.

In Appendix 1, we will derive a technique for solving this equation system using first-order exponential differencing. The result of this appendix is that, if we omit frequency dependence, HZ(I,J) is advanced according to

$$HZ(I,J)^{n+1} = e^{-\mu_\infty^{-1}\sigma_0^*\Delta t} HZ(I,J)^n - (1 - e^{-\mu_\infty^{-1}\sigma_0^*\Delta t})(\sigma_0^*)^{-1}J_z^{T*}(I,J)^{n+1/2} \qquad (20)$$

and [E(I,J)] is advanced according to

$$[E(I,J)]^{n+1/2} = e^{-[\epsilon_\infty]^{-1}[\sigma_0]\Delta t}[E(I,J)]^{n-1/2}$$

$$- ([I] - e^{-[\epsilon_\infty]^{-1}[\sigma_0]\Delta t})[\sigma_0]^{-1}[J^T(I,J)]^n \qquad (21)$$

(The complication of frequency dependence will be considered later.)

As we have said, $[\sigma_0]$ is permitted to be anisotropic. In the actual code, it is represented by a total of five arrays:
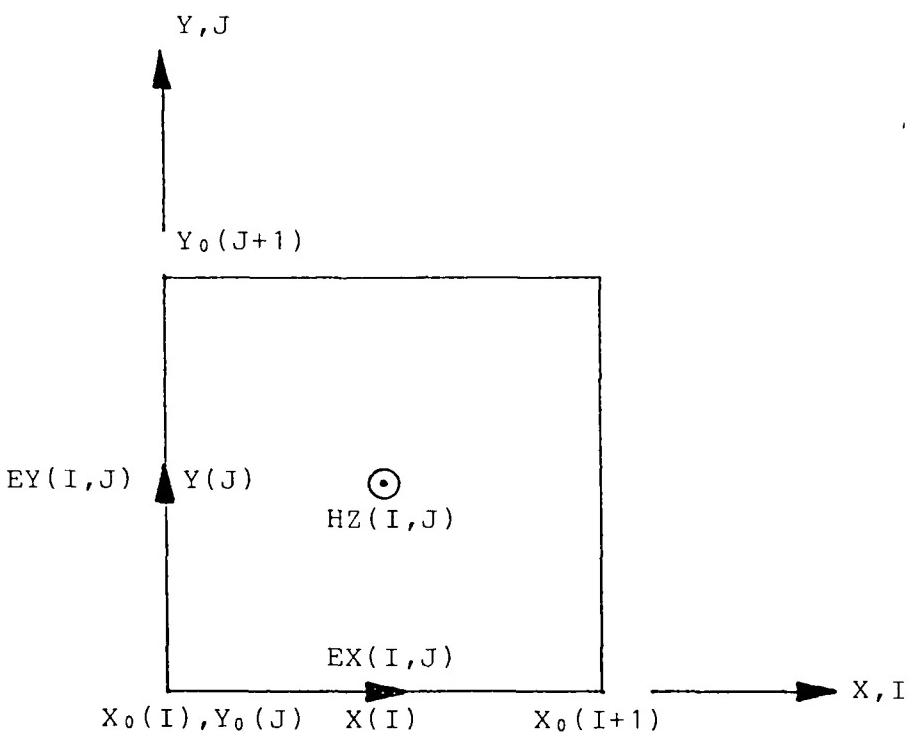
Figure 14. Location of field components in a
unit cell.

SGX(I,J) is the bulk value characterizing the xx component of the conductivity tensor at cell (I,J)

SGY(I,J) is the bulk value characterizing the yy component of the conductivity tensor at cell (I,J)

SGXY(I,J) is the bulk value characterizing the xy and yx components of the conductivity tensor at cell (I,J) (gyrotropic materials are not permitted in the present code)

SGCX(I,J) is the surface conductivity in the x direction on the y-facing surface of cell (I,J)

SGCY(I,J) is the surface conductivity in the y direction of the x-facing surface of cell (I,J)

Thus, the actual conductivity seen by E_x at cell (I,J) is given by

$$\sigma_0(I,J)_{xx} = (SGX(I,J-1) + SGX(I,J))/2 + SGCX(I,J) \tag{22}$$

$$\sigma_0(I,J)_{xy} = (SGXY(I,J-1) + SGXY(I,J))/2 \tag{23}$$

$$\sigma_0(I,J)_{yx} = (SGXY(I,J-1)^{-1} + SGXY(I,J)^{-1})^{-1} \cdot 2 \tag{24}$$

$$\sigma_0(I,J)_{yy} = (SGY(I,J-1)^{-1} + SGY(I,J)^{-1})^{-1} \cdot 2 \tag{25}$$

This arrangement occurs because J_x sees the xx and xy conductivities in parallel, while J_y sees the yx and yy conductivities in series.

The conductivity matrix for E_y at cell (I,J) is analogously described

$$\sigma_0(I,J)_{xx} = (SGX(I-1,J)^{-1} + SGX(I,J)^{-1})^{-1} \cdot 2 \tag{26}$$

$$\sigma_0(I,J)_{xy} = (SGXY(I-1,J)^{-1} + SGXY(I,J)^{-1})^{-1} \cdot 2 \tag{27}$$

$$\sigma_0(I,J)_{yx} = (SGXY(I-1,J) + SGXY(I,J))/2 \tag{28}$$

$$\sigma_0(I,J)_{yy} = (SGY(I-1,J) + SGY(I,J))/2 + SGCY(I,J) \tag{29}$$

Note that, although the physical conductivity tensor is symmetric at each cell ($SGXY(I,J) = SGYX(I,J)$), the mathematical conductivity just described is not symmetric ($\sigma_0(I,J)_{xy} \neq \sigma_0(I,J)_{yx}$).

The dielectric properties of the scatterer are represented by five analogous arrays, EPX, EPY, EPXY, EPCX and EPCY. These are combined in the same way to form the mathematical permittivities $\epsilon_\infty(I,J)_{ij}$ at the E_x and E_y evaluation points of cell (I,J).

Due to the anisotropic cross-terms, it is necessary to know E_y at the E_x evaluation points. This is done by simple linear interpolation,

$$EY(I,J)_x = (EY(I,J) + EY(I+1,J) + EY(I,J-1) + EY(I+1,J-1))/4 \tag{30}$$

E_x at the E_y evaluation points, $EX(I,J)_y$ is obtained the same way. The matrix difference equation (21) is then solved twice at each cell and each time step, once centered at and to advance $EX(I,J)$, and once centered at and to advance $EY(I,J)$.

The following notation is also used:

$QXX(I,J)$ is the (1, 1) component of $e^{-[\epsilon_\infty]^{-1}[\sigma_0]\Delta t}$ evaluated at the E_x points

$QXY(I,J)$ is the (1, 2) component of $e^{-[\epsilon_\infty]^{-1}[\sigma_0]\Delta t}$ evaluated at the E_x points

$QYX(I,J)$ is the (2, 1) component of $e^{-[\epsilon_\infty]^{-1}[\sigma_0]\Delta t}$ evaluated at the E_y points

$QYY(I,J)$ is the (2, 2) component of $e^{-[\epsilon_\infty]^{-1}[\sigma_0]\Delta t}$ evaluated at the E_y points

$SXX(I,J)$, $SXY(I,J)$, $SYX(I,J)$ and $SYY(I,J)$ are $([I] - e^{-[\epsilon_\infty]^{-1}[\sigma_0]\Delta t})[\sigma_0]^{-1}$ correspondingly located and defined.

Additionally, if we refer back to eqs. (15) - (17),

$TAUXX(I,J)$, $TAUXY(I,J)$, $TAUYX(I,J)$ and $TAUYY(I,J)$ are $[\sigma_0]^{-1}[\epsilon_\infty - \epsilon_0]$ analogously located and defined, and

$RXX(I,J)$, $RXY(I,J)$, $RYX(I,J)$ and $RYY(I,J)$ are $[\sigma_0]^{-1}[\sigma_0 - \sigma_b]$ analogously located and defined.

It is necessary to evaluate both components of $[E^S]$ as given in eq. (11) at both E_x and E_y points in each cell. The above conventions indicate how to combine the σ_0 and ϵ_∞ tensors for an inhomogeneous scatterer so this complete set of evaluations may be achieved. In particular, we denote E_{xy}^S as E_y^S evaluated at the E_x mesh point and E_{yx}^S as E_x^S evaluated at the E_y mesh point.

Thus, $E_{xx}^S(I,J)$ is, from eq. (11),

26

$$E_{xx}^S(I,J) = - \text{TAUXX}(I,J)\dot{E}_{xx}^{inc}(I,J) - \text{TAUXY}(I,J)\dot{E}_{xy}^{inc}(I,J)$$

$$- \text{RXX}(I,J)E_{xx}^{inc}(I,J) - \text{RXY}(I,J)E_{xy}^{inc}(I,J) \tag{31}$$

where $E_{xx}^{inc}(I,J)$ is the analytically specified E_x^{inc} field evaluated at E_x mesh points, and $E_{xy}^{inc}(I,J)$ is the analytically specified E_y^{inc} field evaluated at E_x mesh points. Additionally, $E_{yy}^S(I,J)$ is

$$E_{yy}^S(I,J) = - \text{TAUYY}(I,J)\dot{E}_{yy}^{inc}(I,J) - \text{TAUYX}(I,J)\dot{E}_{yx}^{inc}(I,J)$$

$$- \text{RYY}(I,J)E_{yy}^{inc}(I,J) - \text{RYX}(I,J)E_{yx}^{inc}(I,J) \tag{32}$$

where $E_{yy}^{inc}(I,J)$ is the analytically specified E_y^{inc} field evaluated at the E_y mesh points and $E_{yx}^{inc}(I,J)$ is the analytically specified E_x^{inc} field evaluated at the E_x mesh points. Finally, $E_{xy}^S(I,J)$ and $E_{yx}^S(I,J)$ are, in analogy with eq. (30),

$$E_{xy}^S(I,J) = (E_{yy}^S(I,J) + E_{yy}^S(I+1,J) + E_{yy}^S(I,J-1) + E_{yy}^S(I+1,J-1))/4 \tag{33}$$

$$E_{yx}^S(I,J) = (E_{xx}^S(I,J) + E_{xx}^S(I,J+1) + E_{xx}^S(I-1,J) + E_{xx}^S(I-1,J+1))/4 \tag{34}$$

It is also necessary to evaluate both components of $[J^T]$ as given in eq. (9) at both E_x and E_y points in each cell. Using the same convention as above, we let J_{xy}^T be J_y^T evaluated at the E_x points and J_{yx}^T be J_x^T evaluated

27

at the E_y points. Then equation (21), where $[J^T]$ is actually required, uses $[J^T]$ in the form

$$[\sigma_0]^{-1}[J^T] = - [E^S] + [\sigma_0]^{-1}[J_f] - [\sigma_0]^{-1}[\nabla \times H^{scat}] \qquad (35)$$

We have already described how to find the $[E^S]$ contribution to $[J^T]$. It is easy to evaluate $[\sigma_0]^{-1}[J_f]$ because J_f is a prescribed analytic forcing term which can readily be evaluated at either the E_x or the E_y points. The troublesome term is $[\nabla \times H^{scat}]$. This will have both an x and a y component, each of which must be evaluated at the E_x and the E_y points.

Let us designate $(\nabla \times \underline{H}^{scat})_{xx}$ as the x-component of this term evaluated at the E_x points:

$$(\nabla \times \underline{H}^{scat})_{xx} = \frac{HZ(I,J) - HZ(I,J-1)}{Y(J) - Y(J-1)} \qquad (36)$$

The y-component evaluated at an E_x point is

$$(\nabla \times \underline{H}^{scat})_{xy} =$$

$$- \frac{1}{2}\left[\frac{(HZ(I+1,J) + HZ(I+1,J-1)) - (HZ(I,J) + HZ(I,J-1))}{2(X(I+1) - X(I))}\right.$$

$$+ \left.\frac{(HZ(I,J) + HZ(I,J-1)) - (HZ(I-1,J) + HZ(I-1,J-1))}{2(X(I) - X(I-1))}\right] \qquad (37)$$

The y component evaluated at an E_y point is

$$(\nabla \times \underline{H}^{scat})_{yy} = - \frac{HZ(I,J) - HZ(I-1,J)}{X(I) - X(I-1)} \qquad (38)$$

28

and the x component evaluated at an E_y point is

$$(\nabla \times \underline{H}^{scat})_{yx} =$$

$$\frac{1}{2}\left[\frac{(HZ(I,J+1) + HZ(I-1,J+1)) - (HZ(I,J) + HZ(I-1,J))}{2(Y(J+1) - Y(J))}\right.$$

$$\left. + \frac{(HZ(I,J) + HZ(I-1,J)) - (HZ(I,J-1) - HZ(I-1,J-1))}{2(Y(J) - Y(J-1))}\right] \tag{39}$$

Consequently, for example, eq. (21) for advancing $EX(I,J)$ in all its glory, becomes

$$EX(I,J)^{n+1/2} = QXX(I,J)EX(I,J)^{n-1/2} + QXY(I,J)EY(I,J)_x^{n-1/2}$$

$$+ (1 - QXX(I,J))E_{xx}^S(I,J)^n - QXY(I,J)E_{xy}^S(I,J)^n$$

$$- SXX(I,J)(J_f(I,J)_{xx}^n - (\nabla \times \underline{H}^{scat})_{xx}^n)$$

$$- SXY(I,J)(J_f(I,J)_{xy}^n - (\nabla \times \underline{H}^{scat})_{xy}^n) \tag{40}$$

where QXX and QXY are defined after eq. (30), $EY(I,J)_x$ is defined by eq. (30), $E_{xx}^S(I,J)$ is defined by eq. (31), $E_{xy}^S(I,J)$ is defined by eq. (33), SXX and SXY are defined after eq. (30), $J_f(I,J)_{xx}$ and $J_f(I,J)_{xy}$ are the forcing currents, $(\nabla \times \underline{H}^{scat})_{xx}$ is defined by eq. (36), and $(\nabla \times \underline{H}^{scat})_{xy}$ is defined by eq. (37).

The scalar equations for advancing HZ(I,J), eq. (20), is much easier to implement than the matrix equation for advancing [E(I,J)]. We now need to define

XMUZ(I,J) as the bulk permeability at cell (I,J), μ_∞ of eq. (4),

SGMZ(I,J) as the bulk magnetic conductivity at cell (I,J), σ_0^* of eq. (4),

$$QMZZ(I,J) = e^{-XMUZ(I,J)^{-1} \cdot SGMZ(I,J) \cdot \Delta t} \tag{41}$$

$$SMZZ(I,J) = (1 - QMZZ(I,J))/SGMZ(I,J) \tag{42}$$

$$TAUMZZ(I,J) = \sigma_0^{*-1}(\mu_\infty - \mu_0) \tag{43}$$
evaluated at the center of cell (I,J), and

$$RMZZ(I,J) = \sigma_0^{*-1}(\sigma_0^* - \sigma_b^*) \tag{44}$$
also evaluated at the center of cell (I,J)

The murderously complicated interpolations involved in advancing $\underline{E}$ do not occur in advancing H_z partly because H_z is the only component of $\underline{H}$ present, and partly because H_z is evaluated at the center, not on an edge of the cell.

From eq. (10), $H_{zz}^S(I,J)$ is then

$$H_{zz}^S(I,J) = - TAUMZZ(I,J)\dot{H}_{zz}^{inc}(I,J) - RMZZ(I,J)H_{zz}^{inc}(I,J) \tag{45}$$

where $H_{zz}^{inc}(I,J)$ is the analytically specified H_z^{inc} field evaluated at the cell centers.

One also need only evaluate $J_z^{*T}(I,J)$ of eq. (8) at the cell centers. Equation (20), where $J_z^{*T}(I,J)$ actually appears, uses the form

30

$$(\sigma_0^*)^{-1} J_z^{*T}(I,J) = -H_{zz}^S(I,J) + (\sigma_0^*)^{-1} J_f^*(I,J)_{zz}$$

$$+ (\sigma_0^*)^{-1}(\nabla \times \underline{E}^{scat})_{zz} \tag{46}$$

Here, we already have found $H_{zz}^S(I,J)$, $J_f^*(I,J)_{zz}$ is a prescribed magnetic current density (which would be zero on any physically real problem), and $(\nabla \times \underline{E}^{scat})_{zz}$ is just

$$(\nabla \times \underline{E}^{scat})_{zz} = \frac{EY(I+1,J) - EY(I,J)}{X_0(I+1) - X_0(I)} - \frac{EX(I,J+1) - EX(I,J)}{Y_0(J+1) - Y_0(J)} \tag{47}$$

Thus, eq. (20) for advancing $HZ(I,J)$ becomes

$$HZ(I,J)^{n+1} = QMZZ(I,J)HZ(I,J)^n + (1 - QMZZ(I,J))H_{zz}^S(I,J)^{n+1/2}$$

$$- SMZZ(I,J)(J_f^*(I,J)_{zz}^{n+1/2} + (\nabla \times \underline{E}^{scat})_{zz}^{n+1/2}) \tag{48}$$

Introduction of Frequency Dependence

Let us assume the frequency-dependent term in Eq. (19) has a kernel of the form

$$\underline{\underline{K}}(\mu) = \sum_{m=1}^{M} \underline{\underline{a}}_m e^{-\beta_m \mu} \tag{49}$$

where $\underline{\underline{a}}_m$ has the units of conductivity. This assumption is equivalent to expanding the frequency-dependence of the material's electrical properties in a Prony series under the constraint that all the poles be on the real axis. (Appendix 1 indicates how one may relax the real-poles-only constraint.)

Equation (19) then becomes

$$\underline{\underline{\epsilon}}_\infty \cdot \frac{\partial \underline{E}^{scat}}{\partial t} + \underline{\underline{\sigma}}_0 \cdot \underline{E}^{scat} + \sum_{m=1}^{M} \underline{\underline{a}}_m \cdot \underline{J}_m^{scat} = - \underline{J}^T \tag{50}$$

where

$$\underline{J}_m^{scat}(t) = e^{-\beta_m t} \int_\infty^t \frac{\partial \underline{E}^{scat}(t')}{\partial t'} e^{\beta_m t'} dt' \tag{51}$$

In eq. (50), $\underline{J}^T$ is still given by eq. (35), but with the understanding that $\underline{E}^S$ has the frequency-dependent term restored. In other words, $\underline{E}^S$ is now represented by eq. (11), not eqs. (31) and (32).

The $\underline{J}_m^{scat}$ of eq. (50) are not clearly identifiable either as conduction or as displacement currents. We shall coin the name "Prony currents" for them. Equation (50) for $\underline{J}_m^{scat}(t)$ is much easier to recognize if we differentiate it once; its homogeneous solution is just a decaying exponential:

$$\frac{\partial \underline{J}_m^{scat}}{\partial t} + \beta_m \underline{J}_m^{scat} = \frac{\partial \underline{E}^{scat}}{\partial t} \tag{52}$$

In the 2D TM case, the components of eqs. (50) and (52) then comprise $2(M+1)$ coupled first-order differential equations for $\underline{E}^{scat}$ and $\underline{J}_m^{scat}$. Ideally, these equations should all be advanced from $(n-1/2)\Delta t$ to $(n+1/2)\Delta t$ simultaneously each cycle. A technique for doing this is also described in Appendix 1.

However, the present code actually implements a slightly less accurate algorithm where $\underline{E}^{scat}$ alone is advanced first in each cycle, and then the $\underline{J}_m^{scat}$ are advanced separately. Finally, a correction is made to the advanced $\underline{E}^{scat}$ to account for the effects of the $\underline{J}_m$.

At this point, it is most instructive to go back to eq. (7) and perform a rearrangement:

$$\nabla \times \underline{H}^{scat} = \underline{\underline{\epsilon}}_\infty \cdot \frac{\partial \underline{E}^{scat}}{\partial t} + \underline{\underline{\sigma}}_0 \cdot \underline{E}^{scat} + (\underline{\underline{\epsilon}}_\infty - \underline{\underline{I}}\epsilon_0) \cdot \frac{\partial \underline{E}^{inc}}{\partial t}$$

$$+ (\underline{\underline{\sigma}}_0 - \underline{\underline{I}}\sigma_b) \cdot \underline{E}^{inc} + \int_{-\infty}^t \underline{\underline{K}}(t-t') \cdot \frac{\partial \underline{E}^T(t')}{\partial t'} + \underline{J}_f \tag{53}$$

The inhomogeneous part of this equation can be written

$$[J^T] + [J^P] = - [\sigma_0][E^S] + [J^P] + [J_f] - [\nabla \times \underline{H}^{scat}] + [J^P] \tag{54}$$

where $[E^S]$ and $[J^P]$ are

$$[E^S] = - [\tau][\dot{E}^{inc}] - [R][E^{inc}] \tag{55}$$

33

$$[J^P] = \int_{-\infty}^{t} [K(t-t')][\dot{E}^T(t')]dt' \qquad (56)$$

with $[\tau]$ and $[R]$ still respectively given by eqs. (15) and (16).

Substituting eqs. (54)-(56) back into (53) then results in

$$\underline{\underline{\epsilon}}_\infty \cdot \frac{\partial \underline{E}^{scat}}{\partial t} + \underline{\underline{\sigma}}_0 \cdot \underline{E}^{scat} = - \underline{J}^T - \underline{J}^P \qquad (57)$$

This equation is just (19) with the frequency-dependent term transferred to the right and represented as $\underline{J}^P$. It is advanced according to eq. (21):

$$[E(I,J)]^{n+1/2} = e^{-[\epsilon_\infty]^{-1}[\sigma_0]\Delta t}[E(I,J)]^{n-1/2}$$

$$- ([I] - e^{-[\epsilon_\infty]^{-1}[\sigma_0]\Delta t})[\sigma_0]^{-1}[J^T(I,J) + J^P(I,J)]^n \quad (58)$$

The problem with direct application of this procedure is that we do not know the portion of $\underline{J}^P$ associated with $\underline{\dot{E}}^{scat}$ at $n\Delta t$ until we have advanced the Prony currents, and we cannot, strictly speaking, do that until we have advanced $\underline{E}^{scat}$.

As mentioned previously, the code does not presently utilize the procedure described in Appendix 1 for simultaneous advancement of $\underline{E}^{scat}$ and $\underline{J}_m^{scat}$. Rather, we first find an intermediate value of $\underline{E}^{scat}$ obtained with effects of the Prony currents omitted:

$$[E(I,J)]^{int} = e^{-[\epsilon_\infty]^{-1}[\sigma_0]\Delta t}[E(I,J)]^{n-1/2}$$

$$- ([I] - e^{-[\epsilon_\infty]^{-1}[\sigma_0]\Delta t})[\sigma_0]^{-1}[J^T(I,J)]^n \tag{59}$$

The procedure for obtaining this intermediate value is identical to the procedure described in the previous section for advancement through a total cycle in the absence of frequency-dependent effects. Its implementation in the code is also identical to what was described in the previous section.

Let us next turn to the advancement of the total Prony current $\underline{J}^P$ as given by eqs. (49) and (56):

$$\underline{J}^P = \sum_{m=1}^{M} \underline{\underline{a}}_m \cdot \underline{J}_m^T \tag{60}$$

where

$$\underline{J}_m^T(t) = e^{-\beta_m t} \int_{-\infty}^{t} \frac{\partial \underline{E}^T(t')}{\partial t'} e^{\beta_m t'} dt' \tag{61}$$

Equation (61), like (51), is made more recognizable by differentiating with respect to time:

$$\frac{\partial \underline{J}_m^T}{\partial t} + \beta_m \underline{J}_m^T = \frac{\partial \underline{E}^T}{\partial t} = \frac{\partial(\underline{E}^{inc} + \underline{E}^{scat})}{\partial t} \tag{62}$$

The equation for exponential-difference advancement of this result is

$$\underline{J}_m^T(I,J)^{n+1/2} = e^{-\beta_m \Delta t} \underline{J}_m^T(I,J)^{n-1/2}$$

$$+ (1 - e^{-\beta_m \Delta t})(\underline{\dot{E}}^{inc}(I,J) + \underline{\dot{E}}^{scat}(I,J))^n / \beta_m \qquad (63)$$

The incident field $\underline{\dot{E}}^{inc}$ is a specified analytic function. At present, the code evaluates $\underline{\dot{E}}^{scat}(I,J)^n$ as

$$\underline{\dot{E}}^{scat}(I,J)^n = \frac{\underline{E}(I,J)^{int} - \underline{E}(I,J)^{n-1/2}}{\Delta t} \qquad (64)$$

Equations (63) and (64) may be combined to give an expression for $\underline{J}_m^T(I,J)^{n+1/2}$ in terms of known quantities. We can then determine $\underline{J}^P(I,J)^n$ as

$$\underline{J}^P(I,J)^n = \sum_{m=1}^{M} [a_m(I,J)][J_m^T(I,J)^{n+1/2} + J_m^T(I,J)^{n-1/2}]/2 \qquad (65)$$

Subtraction of eq. (59) from eq. (58) then permits us to advance $[E(I,J)]$ from its intermediate value to its value at the new time step, $(n+1/2)\Delta t$:

$$[E(I,J)]^{n+1/2} = [E(I,J)]^{int}$$

$$- ([I] - e^{-[\epsilon_\infty]^{-1}[\sigma_0]\Delta t})[\sigma_0]^{-1}[J^P(I,J)]^n \qquad (66)$$

Frequency dependence in the magnetic properties of the material can be treated in an exactly dual manner to what we have just described for the electrical properties.

36

At present, we have not coded up magnetic frequency dependence, nor have we combined frequency dependence with off-diagonal type anisotropy. Both these generalizations would be perfectly obvious extensions of what has been done, but we cannot conceive a cannonical problem we could check the results against.

Not mixing off-diagonal anisotropy and frequency dependence means we only treat diagonal $\underline{\underline{a}}_m$ tensors. If eq. (65) is substituted in eq. (66), we obtain

$$[E(I,J)]^{n+1/2} = [E(I,J)]^{int} - ([I] - e^{-[\epsilon_\infty]^{-1}[\sigma_0]\Delta t})$$

$$\cdot \sum_{m=1}^{M} [SA_m(I,J)][J_m^T(I,J)^{n+1/2} + J_m^T(I,J)^{n-1/2}] \tag{67}$$

where

$$[SA_m(I,J)] = [\sigma_0(I,J)]^{-1}[A_m(I,J)] \tag{68}$$

In the actual code, two arrays are used to describe the material effects of each term in the Prony series. Let $\sigma_0(I,J)^{-1}_{xx}$ represent the xx element of the inverse of the matrix described by eqs. (22)-(25) at cell (I,J). Let $\sigma_0(I,J)^{-1}_{yy}$ similarly represent the yy element of the inverse of the matrix described by eqs. (26)-(29) at cell (I,J).

Moreover, let AAMX(I,J) represent the xx element of the mth Prony tensor of the bulk material at cell (I,J), and let AAMY(I,J) represent the corresponding yy element. Then the xx element of $[SA_m(I,J)]$ which actually relates the x component of $\underline{J}_m^T(I,J)$ to the x component of $\underline{E}(I,J)$ is called

37

$$SAMX(I,J) = \sigma_0(I,J)_{xx}^{-1} \ (AAMX(I,J-1) + AAMX(I,J))/2 \qquad (69)$$

Similarly, the yy element of $[SA_m(I,J)]$ which actually relates the y component $\underline{J}_m^T(I,J)$ to the y component of $\underline{E}(I,J)$ is called

$$SAMY(I,J) = \sigma_0(I,J)_{yy}^{-1} \ (AAMY(I-1,J) + AAMY(I,J))/2 \qquad (70)$$

In keeping with our simplification of not mixing off-diagonal anisotropy with frequency dependence, we ignore any possible off-diagonal nonzero values in $[SA_m(I,J)]$.

It turns out that only $SAMX(I,J)$ and $SAMY(I,J)$ need actually be stored. That is, it is not necessary to assign arrays for keeping $\sigma_0(I,J)_{xx}^{-1}$, $\sigma_0(I,J)_{yy}^{-1}$, $AAMX(I,J)$ and $AAMY(I,J)$.

Consequently, the actual equation used in the code for implementing the x-component of the Prony correction is

$$EX(I,J)^{n+1/2} = EX(I,J)^{int}$$

$$- (1 - QXX(I,J)) \ \sum_{m=1}^{M} SAMX(I,J) \ XJMSX(I,J)^n \qquad (71)$$

where

$$XJMX(I,J)^n = [J_m^T(I,J)_x^{n+1/2} + J_m^T(I,J)_x^{n-1/2}]/2 \qquad (72)$$

Similarly, the actual equation used for implementing the y-component of the Prony correction is

$$EY(I,J)^{n+1/2} = EY(I,J)^{int}$$

$$- (1 - QYY(I,J)) \sum_{m=1}^{M} SAMY(I,J) \ XJMY(I,J)^{n} \qquad (73)$$

where

$$XJMY(I,J)^{n} = [J_m^T(I,J)_y^{n+1/2} + J_m^T(I,J)_y^{n-1/2}]/2 \qquad (74)$$

Transformation from the Near-field Time Domain to the
Far-field Frequency Domain

The foregoing work described the determination of the scatterer's electromagnetic response and associated near fields. We are actually interested in the RCS, which is a far-field quantity. Now we shall describe how the code extracts the RCS from the near-field results. In this process, we also transform from time domain to frequency domain.

Any electromagnetic field can be expressed in terms of an electric and a magnetic vector potential, $\underline{A}$ and $\underline{A}^*$. These vector potentials (in the frequency domain) obey the inhomogeneous wave equations.

$$\nabla^2 \underline{A} + k^2 \underline{A} = -\mu_0 \underline{J} \tag{75}$$

$$\nabla^2 \underline{A}^* + k^2 \underline{A}^* = \epsilon_0 \underline{J}^* \tag{76}$$

Here $\underline{J}^*$ is the fictitious magnetic current density often found useful in manipulating Maxwell's equations. Equations (75) and (76) can be generalized to apply to any linear medium, although we shall find their free-space form adequate for our uses.

In 2D, we define the far field to be the region where all fields drop off as $r^{-1/2}$; i.e., where all the faster falling terms have vanished. We can then separate the electric and magnetic fields into two parts,

$$\underline{E} = \underline{E}_e + \underline{E}_m \tag{77}$$

$$\underline{H} = \underline{H}_e + \underline{H}_m \tag{78}$$

The e-subscripted parts are associated with the electric vector potential $\underline{A}$, and the m-subscripted parts are associated with the magnetic vector potential $\underline{A}^*$. In particular, if we call Y_0 and Z_0 the admittance and impedance of free space, we can show in the far field that

$$\underline{H}_e = \nabla \times \underline{A}/\mu_0 = i\omega Y_0 \underline{i}_r \times \underline{A} \tag{79}$$

$$\underline{E}_m = \nabla \times \underline{A}^*/\epsilon_0 = i\omega Z_0 \underline{i}_r \times \underline{A}^* \tag{80}$$

$$\underline{E}_e = i\omega \underline{A}_t = i\omega(\underline{i}_\phi A_\phi + \underline{i}_z A_z) \tag{81}$$

$$\underline{H}_m = - i\omega \underline{A}_t^* = - i\omega(\underline{i}_\phi A_\phi^* + \underline{i}_z A_z^*) \tag{82}$$

Here, a t subscript indicates that only the transverse components (ϕ and z) are retained. Equations (79)-(82) are analogous to 3D formulas, and depend on the fact that

$$\frac{e^{i(kr-\omega t)}}{\sqrt{r}} \tag{83}$$

is a valid far-field frequency-domain 2D solution of the wave equation even if the more general

$$\frac{f(t - r/c)}{\sqrt{r}} \tag{84}$$

is not a valid time-domain solution. These equations tell us that if we can evaluate $\underline{A}$ and $\underline{A}^*$, we can find the 2D RCS without undue complication.

41

In two dimensions, the Green's function for the scalar wave equation in the frequency domain obeys

$$\nabla^2 G(\underline{r}|\underline{r}') + k^2 G(\underline{r}|\underline{r}') = \delta(\underline{r}-\underline{r}') \qquad (85)$$

where $\underline{r}$ is the scatterer location and $\underline{r}'$ is the observer location. This equation has solution

$$G(\underline{r}|\underline{r}') = -\frac{i}{4} H_o^{(1)}(kR) \qquad (86)$$

Thus, at least in cartesian coordinates, $\underline{A}$ and $\underline{A}^*$ become

$$\underline{A}(\underline{r}',\omega) = \iint \frac{iH_o^{(1)}(kR)}{4\mu_0} \underline{J}(\underline{r},\omega)d\underline{r} \qquad (87)$$

$$\underline{A}^*(\underline{r}',\omega) = -\iint \frac{iH_o^{(1)}(kR)}{4\epsilon_0} \underline{J}^*(\underline{r},\omega)d\underline{r} \qquad (88)$$

For the far field region, $G(\underline{r}|\underline{r}')$ asymptotically approaches

$$G(\underline{r}|\underline{r}') = \frac{e^{-i3\pi/4}}{4} \sqrt{\frac{2}{\pi kR}} e^{ikR} \qquad (89)$$

This expression may be further manipulated by letting r' replace R in the denominator of the radical. The phase term requires a bit more care:

$$kR \rightarrow k(r' - \underline{i}'_r \cdot \underline{r}) = kr' - (kx \cos\phi' + ky \sin\phi') \qquad (90)$$

42

where

$$\underline{i}_{r'} = \underline{i}_x \cos\phi' + \underline{i}y \, \sin\phi' \qquad (91)$$

is a unit vector pointing from the target to a far-field observer.

Using these expansions, we can rewrite the formula for $\underline{A}$ in the far field as

$$\underline{A}(\underline{r}',\omega) =$$

$$- \frac{\mu_0 e^{-3i\pi/4}}{4} \sqrt{\frac{2}{\pi k r'}} \, e^{ikr'} \iint \underline{J}(\underline{r},\omega) e^{-ik(x \cos\phi' + y \, \sin\phi)} d\underline{r} \qquad (92)$$

A corresponding expression exists for $\underline{A}^*(\underline{r}',\omega)$. The far-field expression for $\underline{E}_e$ then becomes

$$\underline{E}_e(\underline{r}',\omega) = i\omega \, \underline{A}_t(\underline{r}',\omega) =$$

$$- \frac{i\omega\mu_0 e^{-3i\pi/4}}{4} \sqrt{\frac{2}{\pi k r'}} \, e^{ikr'} \iint \underline{J}_t(\underline{r},\omega) e^{-ik(x \cos\phi' + y \, \sin\phi')} d\underline{r} \qquad (93)$$

Similarly, $\underline{H}_m$ becomes

$$\underline{H}_m(\underline{r}',\omega) = i\omega\underline{A}_t^*(\underline{r}',\omega) =$$

$$\frac{i\omega\epsilon_0 e^{-3i\pi/4}}{4}\sqrt{\frac{2}{\pi k r'}}\ e^{ikr'}\iint \underline{J}_t^*(\underline{r},\omega)e^{-ik(x\cos\phi' + y\sin\phi')}d\underline{r} \qquad (94)$$

Analogous formulas exist for $\underline{E}_m$ and $\underline{H}_e$.

Equations (93) and (94) are not directly applicable to the output of our 2D Maxwell solver as these equations demand the frequency-domain $\underline{J}$ and $\underline{J}^*$, while the Maxwell solver outputs the time-domain currents.

Let us say we want $\underline{E}_e(\underline{r}',\omega_q)$ where ω_q is one of N_q discrete frequencies of interest. We can then write

$$\underline{E}_e(\underline{r}',\omega_q) = -\frac{i\omega_q\mu_0 e^{-3i\pi/4}}{8\pi}\sqrt{\frac{2}{\pi k_q r'}}\ e^{ik_q r'}\ \cdot$$

$$\int_{-\infty}^{\infty} e^{j\omega_q t}\ dt \iint \underline{J}_t(\underline{r},t)e^{i\underline{k}_q' \cdot \underline{r}}\ d\underline{r} \qquad (95)$$

where $\underline{k}_q'$ is the wavenumber pointing towards the observer at ω_q and where we have interchanged the order of time and space integration after replacing $\underline{J}_t(\underline{r},\omega)$ with its inverse Fourier representation.

Analogously, $\underline{H}_m(\underline{r}',\omega_q)$ becomes

$$\underline{H}_m(\underline{r}',\omega_q) = \frac{i\omega_q\epsilon_0 e^{-3i\pi/4}}{8\pi}\sqrt{\frac{2}{\pi k_q' r'}}\ e^{ik_q r'}\ \cdot$$

$$\int_{-\infty}^{\infty} e^{j\omega_q t} \, dt \iint \underline{J}_t^*(\underline{r},t) e^{-i\underline{k}'_q \cdot \underline{r}} \, d\underline{r} \tag{96}$$

Equations (95) and (96), and the two companion equations for $\underline{E}_m$ and $\underline{H}_e$ are in a form which is compatible with our time-domain Maxwell solver. Taking the time integration outside the space integration is vitally important to the efficiency of our algorithm. Were this not done, $\underline{J}_t(\underline{r},t)$ and $\underline{J}_t^*(\underline{r},t)$ would have to be Fourier transformed at every point before being integrated over space. The form of eqs. (95) and (96) replaces this enormous computation with a single Fourier transform on the result of the space integral.

If we let $\underline{J}^{scat}$ represent the total current (conduction, displacement and Prony) associated with the scattered electromagnetic field (see eq. (53))

$$\underline{J}^{scat} = \underline{\underline{\epsilon}}_\infty \cdot \frac{\partial \underline{E}^{scat}}{\partial t} + \underline{\underline{\sigma}}_0 \cdot \underline{E}^{scat} + (\underline{\underline{\epsilon}}_\infty - \underline{\underline{I}}\epsilon_0) \cdot \frac{\partial \underline{E}^{inc}}{\partial t}$$

$$+ (\underline{\underline{\sigma}}_0 - \underline{\underline{I}}\sigma_b) \cdot \underline{E}^{inc} + \int_{-\infty}^{t} \underline{\underline{K}}(t-t') \cdot \frac{\partial \underline{E}^T(t')}{\partial t'} \, dt' \tag{97}$$

and if we substitute $\underline{J}_t^{scat}$ for $\underline{J}_t$ in eq. (95), $\underline{E}_e$ of eq. (95) becomes the scattered field $\underline{E}^{scat}$ of the first section unless magnetic materials are present. That is, $\underline{J}_t^{scat}$ integrated over the scatterer cross-section according to eq. (95) gives $\underline{E}^{scat}$ in the absence of magnetic materials.

$$RCS(\omega_q) = 2\pi \left| \frac{\underline{E}_e^{scat}(\underline{r}',\omega_q) \cdot \sqrt{r'}}{\underline{E}^i(r',\omega_q)} \right|^2 \tag{98}$$

In this convention, $\underline{A}^*$ and $\underline{E}_m$ are zero.

45

However, it is possible to replace the area integral of eqs. (95) and (96) with a contour integral by means of Huygens principle. In particular, let S be a closed contour which completely surrounds the target. (For instance, let S be a rectangle defined by $x = x_1, x_2$ and $y = y_1, y_2$.) Let $\underline{E}^{scat}$ and $\underline{H}^{scat}$ be the scattered fields which our Maxwell solver predicts will exist on S due to the time-domain illumination. Let $\underline{n}$ be an outward-pointing unit normal on S. If we then remove the scatterers and its currents, but let an electric surface current

$$\underline{K} = \underline{n} \times \underline{H}^{scat} \tag{99}$$

and a magnetic surface current

$$\underline{K}^* = - \underline{n} \times \underline{E}^{scat} \tag{100}$$

flow on S, the scattered electromagnetic field will be replicated outside S. This means the area integral of eq. (95) may be replaced by

$$\sum_p (\underline{n} \times \underline{H}^{scat}(\underline{r}_p, t))_t e^{-i\underline{k}'_q \cdot \underline{r}_p} \Delta s_p = \underline{I}_q^{scat}(t)_t \tag{101}$$

where the summation over p represents integration over the finite difference cell edges which lie on S. This summation is represented by I because it has the dimension of amperes. In the actual code, it goes by the name $XIEST_q$.

Analogously, the area integral present in eq. (96) for $\underline{H}_m(\underline{r}, \omega_q)$ can be written

$$\sum_p \left(-\underline{n} \times \underline{E}^{scat}(\underline{r}_p, t)\right)_t e^{-i\underline{k}'_q \cdot \underline{r}_p} \Delta s_p = \underline{I}^{scat}_q(t)^*_t \qquad (102)$$

(Remember the t subscript on $\underline{I}$, $\underline{I}^*$, or anything else implies evaluation with the r component omitted.) In the code, this variable is called $XIMST_q$.

Equations (95) and (101) indicate the z-component of $\underline{H}^{scat}$ is associated with the ϕ-component of $\underline{E}_e(\underline{r}', \omega_q)$. The ϕ-component of $\underline{E}^{scat}$ in eq. (102) has the same association, as the cross with $\underline{i}_r$ in eq. (80) proves. These scattered fields are the TM solution.

Analogously, the ϕ-component of $\underline{H}^{scat}$ in eq. (101) and the z-component of $\underline{E}^{scat}$ in eq. (102) relate to the (decoupled) TE solution, which we are not treating in detail at this time.

Let us use $\underline{I}^{scat}_q(t)^n_t$ to denote this "current" evaluated from the finite-difference code at $n\Delta t$. Let us analogously denote $\underline{I}^{scat}_q(t)^{*n+1/2}_t$. As the finite-difference calculation progresses, we can then keep running summations for each frequency ω_q,

$$\underline{Q}^{scat}_q(t)^n_t = \sum_{m=1}^{n} \underline{I}^{scat}_q(t)^m_t \, e^{j\omega_q m\Delta t} \Delta t \qquad (103)$$

$$\underline{Q}^{scat}_q(t)^{*n+1/2}_t = \sum_{m=1}^{n} \underline{I}^{scat}_q(t)^{*m+1/2}_t \, e^{j\omega_q (m+1/2)\Delta t} \Delta t \qquad (104)$$

When the time-domain finite difference calculation is complete, these Q's will then respectively contain quantities which are directly proportional to the electric and magnetic contribution to the RCS at ω_q. Note that it is only necessary to backstore $2N_q$ complex quantities during the time-domain finite-difference calculation in order to preserve all the information necessary to generate a monostatic RCS as a function of ω.

The symbol Q is used in eq. (103) because it represents a quantity with units of coulombs. In the code, it is written $SIEST_q$. The scattered electric field associated with $Q_q^{scat}(t)_t$ is

$$\underline{E}_e^{scat}(\underline{r}',\omega_q) = - \frac{i\omega_q\mu_0 e^{-3i\pi/4}}{8\pi} \sqrt{\frac{2}{\pi k_q r'}} e^{ik_q r'} \underline{Q}_q^{scat}(\infty)_t^\infty \qquad (105)$$

The code tracks the ϕ-component of this quantity as $EPES_q$, when $\sqrt{r'}$ is normalized out. Analogously, the scattered magnetic field associated with $\underline{Q}_q^{scat}(t)_t^*$ is

$$\underline{H}_m^{scat}(\underline{r}',\omega_q) = \frac{i\omega_q\epsilon_0 e^{-3i\pi/4}}{8\pi} \sqrt{\frac{2}{\pi k_q r'}} e^{ik_q r'} \underline{Q}_q^{scat}(\infty)_t^{*\infty} \qquad (106)$$

In the code, the z-component of this quantity is $HZMS_q$ when $\sqrt{r'}$ is normalized out. The scattered electric field associated with the magnetic current is obtained by combining eqs. (80) and (106),

$$\underline{E}_m^{scat}(\underline{r}',\omega_q) = \frac{i\omega_q e^{-3i\pi/4}}{8\pi c} \sqrt{\frac{2}{\pi k_q r'}} e^{ik_q r'} \underline{i}_r' \times \underline{Q}_q^{scat}(\infty)^{*\infty} \qquad (107)$$

In the code, the ϕ-component of this quantity, less the $\sqrt{r'}$ factor, is $EPMS_q$.

The radar cross section then becomes

$$RCS(\omega_q) = 2\pi \left| \frac{(\underline{E}_e^{scat}(\underline{r}',\omega_q) + \underline{E}_m^{scat}(\underline{r}',\omega_q))\sqrt{r'}}{\underline{E}^i(\underline{r}',\omega_q)} \right|^2 \qquad (108)$$

48

In the code, $SCATXE_q$ is the E_e^{scat} contribution to the ratio inside the absolute value signs, and $SCATXM_q$ is the E_m^{scat} contributions.

APPENDIX 1.   SOLUTION OF THE TENSOR WAVE EQUATION

Let us consider the case where anisotropy, but not frequency dependence, is present,

$$[\epsilon_\infty] \; D[E] \; + \; [\sigma_0][E] \; = \; [J] \tag{A1}$$

This matrix differential equation has a homogeneous solution

$$[E]_h \; = \; e^{-[\epsilon_\infty]^{-1}[\sigma_0]t} \; [A] \tag{A2}$$

and a particular solution

$$[E]_p \; = \; [\sigma_0]^{-1}[J] \tag{A3}$$

giving a general solution

$$[E] \; = \; e^{-[\epsilon_\infty]^{-1}[\sigma_0]t} \; [A] \; + \; [\sigma_0]^{-1}[J] \tag{A4}$$

The constant vector [A] may be evaluated at $(n - 1/2)\Delta t$:

$$[E]^{n-1/2} \; = \; [A] \; + \; [\sigma_0]^{-1}[J]^n \tag{A5}$$

This gives the new E-field vector in terms of the old,

50

$$[E]^{n+1/2} = e^{-[\epsilon_\infty]^{-1}[\sigma_0]t}[E]^{n-1/2}$$

$$+ \left([I] - e^{-[\epsilon_\infty]^{-1}[\sigma_0]t}\right)[\sigma_0]^{-1}[J]^n \tag{A6}$$

END

DTIC

7-86